



UNIVERSITY OF LEEDS

This is a repository copy of *Surface Fatigue Behaviour of a WC/aC:H Thin-Film and the Tribochemical Impact of Zinc Dialkyldithiophosphate*.

White Rose Research Online URL for this paper:
<https://eprints.whiterose.ac.uk/152265/>

Version: Accepted Version

Article:

Soltanahmadi, S, Charpentier, T, Nedelcu, I et al. (7 more authors) (2019) Surface Fatigue Behaviour of a WC/aC:H Thin-Film and the Tribochemical Impact of Zinc Dialkyldithiophosphate. *ACS Applied Materials & Interfaces*, 11 (44). pp. 41676-41687. ISSN 1944-8244

<https://doi.org/10.1021/acsami.9b14669>

© 2019 American Chemical Society. This is an author produced version of a journal article published in *ACS Applied Materials & Interfaces*. Uploaded in accordance with the publisher's self-archiving policy.

Reuse

Items deposited in White Rose Research Online are protected by copyright, with all rights reserved unless indicated otherwise. They may be downloaded and/or printed for private study, or other acts as permitted by national copyright laws. The publisher or other rights holders may allow further reproduction and re-use of the full text version. This is indicated by the licence information on the White Rose Research Online record for the item.

Takedown

If you consider content in White Rose Research Online to be in breach of UK law, please notify us by emailing eprints@whiterose.ac.uk including the URL of the record and the reason for the withdrawal request.



eprints@whiterose.ac.uk
<https://eprints.whiterose.ac.uk/>

Surface Fatigue Behaviour of a WC/aC:H Thin-film and the Tribochemical Impact of Zinc Dialkyldithiophosphate

Siavash Soltanahmadi^{a*}, Thibaut Charpentier^b, Ileana Nedelcu^c, Vishal Khetan^a, Ardian Morina^a, Helen M. Freeman^b, Andrew P. Brown^b, Rik Brydson^b, Marcel C. P. van Eijk^c and Anne Neville^a

*s.soltanahmadi@leeds.ac.uk

^aiFS, School of Mechanical Engineering, University of Leeds, LS2 9JT, UK

^bSchool of Chemical and Process Engineering, University of Leeds, LS2 9JT, UK

^cSKF Research & Technology Development, 3430 DT Nieuwegein, The Netherlands

1 Abstract

In wind turbine gearboxes, (near-)surface initiated fatigue is attributed to be the primary failure mechanism. In this work, the surface fatigue of a hydrogenated tungsten carbide/amorphous carbon (WC/aC:H) thin-film was tested under severe cyclic tribo-contact using PolyAlphaOlefin (PAO) and PAO + Zinc DialkyldithioPhosphate (ZDDP) lubricants. The film was characterised in terms of its structure and chemistry using X-ray diffraction, analytical Transmission Electron Microscopy (TEM) including Electron Energy Loss Spectroscopy (EELS), as well as X-ray Photoelectron Spectroscopy (XPS). The multilayer carbon thin-film exhibited promising surface fatigue performance showing a slight change in the hybridization state of the aC:H matrix. Dehydrogenation of the thin-film and subsequent transformation of cleaved C-H bonds to non-planar sp^2 carbon rings were inferred from EELS and XPS results. Whilst tribo-induced changes to the aC:H matrix were not influenced by a nanometer-thick ZDDP reaction-film, the rate of oxidation of WC and its oxidation state were affected. Whilst accelerating surface fatigue on a steel surface, the ZDDP-tribofilm protected the WC/aC:H film from surface fatigue. In contrast to the formation of polyphosphates from ZDDP molecules on steel surfaces, it appeared that on the WC/aC:H thin film surface ZDDP molecules decompose to ZnO suppressing the oxidative degradation of WC.

2 Introduction

With the increased demand for renewable energy, the implementation of wind plants has escalated significantly. However, premature failures of the bearings in wind turbine gearboxes

have hindered progress towards enhanced wind turbine efficiency. Micropitting is a surface fatigue phenomenon occurring in wind turbine gearboxes under certain conditions which has become more prevalent over the last fifteen years. Studies have shown that certain anti-wear additives which are essential to mitigate catastrophic wear, actually accelerate micropitting¹. In order to tackle micropitting, approaches such as applying specific surface finishes² and coatings²⁻⁵ as well as improving lubricant performance^{1,6} have all been considered.

A surface coating that can mitigate surface fatigue would enable reliable and environmentally-friendly energy production. Tungsten carbide/amorphous carbon (WC/aC) thin-films show promising micropitting performance²⁻⁵. Depending on the WC concentration alloyed into the aC matrix and the specific deposition parameters, tungsten can chemically react with carbon to form highly disordered amorphous-like phases or, alternatively, crystallites of either cubic β -WC_{1-x}⁷⁻¹¹ or hexagonal α -WC¹² and α -W₂C^{8, 10, 13-14}. This may give rise to different mechanochemical properties⁸ and tribological performance¹⁰. In solely aC thin-films, a reduction in *sp*³ hybridized bonds as a result of changing the bias voltage during deposition can decrease the internal stresses in the film¹⁵. With WC/aC thin-films the internal stresses alter in a more complex manner^{12, 14}. Up to the solubility limit of WC in carbon, intrinsic stresses in the thin-film are reduced. This is attributed to the greater mass of the tungsten ion and its higher momentum which relaxes compressive stresses¹² and the presence of W–C bonds which alleviate strain energy arising from bond angle distortions relative to solely C–C bonds¹⁴. Above the solubility limit, the formation of incoherent interfaces between the aC matrix and precipitated tungsten carbide crystals hinder stress fields through incoherent stress relaxation¹⁶.

In addition to the thin-film properties, lubricant additives influence the tribological performance of aC coated surfaces¹⁷. The impact of lubricant additives on aC thin-films has been studied under sliding conditions¹⁸⁻²⁰ indicating changes in their mechanochemical structure¹⁹. In the literature, there is extensive research on the development and characterisation of lubricious carbon thin-films and their tribochemistry. Superlubricity of a tetrahedral amorphous carbon (taC) lubricated with oleic acid has been attributed to graphene oxide carbonaceous structures at the interface²⁰. However, there has been no detailed review of the influence of lubricant additive on the surface fatigue performance of aC coated surfaces. Mechanistic studies of surface fatigue in aC thin-films and the influence of additives are required to develop thin-films which are compatible with the lubricant chemistry and can simultaneously hinder micropitting.

Various aC thin-films have been shown to suppress wear and/or surface fatigue in sliding and/or sliding-rolling mechanical components^{2-5, 7-10, 17, 20-21}. Our work has investigated three types of thin-films: taC, aC:H and WC/aC:H which were tested in rolling-sliding conditions under the boundary lubrication regime. In the boundary lubrication regime, the lubricant film occasionally collapses at the contact interface leading to micropitting as a result of solid-solid contacts of asperities on the contacting surfaces. While the examined taC and aC:H thin-films underwent severe surface wear/fatigue, WC/aC:H showed promising performance under different test conditions. This current work presents further investigations into the microstructure and chemistry of the WC/aC:H thin-film and the mechanism of surface fatigue under two different Slide-to-Roll Ratios (SRR) of 2% and 10%.

3 Experimental and analysis apparatus

3.1 Surface fatigue tester

The WC/aC:H thin-films were deposited on the surface of AISI 52100 steel substrates through a combined Physical and Chemical Vapour Deposition (PVD and CVD) technique known as a plasma enhanced CVD (PECVD)²². The deposition procedure employed has been described by Strondl et al.²² and more details can be found in the Supporting Information (SI) (section S1.1). The thin-film was a multilayer coating with a concentration gradient of WC across the thin-film (with higher WC concentration at the initial deposition). WC was magnetron sputtered from a W/WC cathode target to a substrate in an argon/acetylene plasma which controls the deposition of the aC:H phase²². A modified PCS Instrument Micropitting Rig (MPR) was used for surface fatigue investigation of WC/aC:H-coated spherical rollers tribo-contacted against uncoated 52100-steel counter-bodies using two different lubricant formulations of PAO as a Base Oil (BO) and PAO+ZDDP (i.e. BO+ZDDP) at a contact pressure of 1.5 GPa. The reliability of the thin-film was further inspected under a higher contact pressure of 2.5 GPa which was above the substrate yield modulus. More details and a schematic diagram of the rig are shown in the SI (sections S1.2 and S1.3).

3.2 X-Ray Diffraction (XRD)

A Phillips X'Pert diffractometer using Cu K α radiation was used to characterise the crystallographic structure of the thin-film in both Bragg-Brentano (BB) and Grazing Incidence (GI) detection geometries. XRD patterns were collected at ambient temperature over a 2 θ range of 15°-85°.

3.3 Optical and electron microscopy

White Light Interferometry (WLI) using a Bruker NPFLEX™ was used to examine the thin-film and steel surfaces following surface fatigue testing. SEM was used at an accelerating voltage of 5 kV in order to image the coated surfaces both prior to and following tribo-contact. Surfaces were ultrasonically cleaned using n-heptane for 3 minutes prior to imaging. A Focused Ion Beam (FIB)-SEM was used to prepare thin cross-sectional lamellas of the pristine and tribo-tested thin-films for TEM. A thin-film lubricated using BO+ZDDP and tribo-tested under a SRR of 2% and contact pressure of 1.5 GPa was selected for TEM lamella preparation. TEM was undertaken using a FEI Titan Themis³ FEG TEM/STEM operated at 300 kV and fitted with high solid angle Super-X energy dispersive X-ray (EDX) for elemental mapping and a Gatan Quantum ER electron energy loss (EEL) spectrometer/filter. Carbon K-edge EEL spectra from both the pristine and tribo-tested thin-film were collected. A power-law model was used to subtract the underlying spectral background and spectra were normalised to the integrated area over a 20 eV energy window with an onset at 282.5 eV^{21, 23}. More details are presented in the SI (section S1.4).

3.4 Surface chemical analysis

The surface chemistry of the tribo-induced reaction-film in the presence of ZDDP and changes in the chemical state of the WC phase at the thin-film surfaces were studied by XPS using a PHI 5000 Versa Probe™ spectrometer (Ulvac-PHI Inc, Chanhassen, MN, USA) fitted with a monochromatic Al K α X-ray source (1486.6 eV). Specimens were sonicated in n-heptane for 3 minutes before analysis in order to minimise residual lubricant on the surface. High Resolution (HR) spectra (0.05 eV/channel for O 1s, P 2p, S 2p, W 4f and C 1s signals and 0.1 eV/channel for Zn 2p) were also acquired from wear tracks at an area with no micropitting and/or severe surface-damage using a beam size of 100 μ m and a power of 23.7 W in fixed analyser transmission mode. Chemical depth profiling through the surface film was achieved by ion beam etching using 2 keV Ar⁺ ions and a 1 μ A current; with these sputtering parameters, 60 s of sputtering was found to etch 4.5 nm of a steel surface [6].

In further experiments, C 1s and C KVV spectra were collected with a dwell time of 50 ms over an area of 300 by 300 μ m both prior to and following tribo-tests using a Thermo Scientific™ K-Alpha⁺ XPS (Al K α X-ray source) in order to assess changes to the hybridisation state and structure of the thin-film as a result of tribo-contact. Following a meticulous cleaning

procedure (presented in the SI-section S1.4), surfaces were sputtered *in-situ* in the XPS chamber with low energy (4 kV), large (approximately 2000 atom) argon clusters over an area of 2 by 2 mm in order to eliminate the surface contamination resulting from air exposure²⁴. CASAXPS software (version 2.3.19, Casa Software Ltd, UK) was used to fit the XPS and XAES spectra using parameters elucidated in the SI (section S1.4). Three tribo conditions were chosen to represent the influence of the additive, the SRR and a contact pressure (discussed in the SI- Section S1.4).

4 Results:

4.1 Structure of the thin-film

Figure 1 (A) (inset) presents GIXRD data at an incidence angle of 2° which shows three broad peaks due to the surface layer that is expected to be an amorphous a-C:H matrix that contains some WC. The peaks are at ~ 36.6°, ~ 61.5° and ~ 73.6° (*d* spacings 0.245, 0.150 and 0.128 nm) are associated with (111), (220) and (311) planes of cubic β -WC_{1-x} respectively. Tungsten carbide XRD reference patterns are given in Figure S1. Although cubic β -WC_{1-x} is normally only stable above the eutectoid point of 2525°C, in magnetron sputtering metastable β -WC_{1-x} can be deposited without transforming to the thermodynamically-stable α -WC phase^{7, 25}. Additional reflections in BBXRD data at ~44° and ~64° arise from the Fe substrate⁷ and the Cr interlayer. Further peaks at ~39°, 59°, 69° and 73° in BBXRD data can be assigned to cubic W and/or α -W₂C (Figure 1(A) and Figure S1). GIXRD measurements were also carried out at different incident angles of 1°, 3°, 5° and 10° and are presented in Figure S2. With increasing angle, a second peak at ~43° became dissociated from the asymmetric peak at ~36.6° shown inset in Figure 1 (A). This peak corresponds to the (200) plane in β -WC_{1-x} which is the more preferred orientation deeper in the film; Baba et al.²⁶ observed a similar result for thin-films with greater alloyed WC concentration. The appearance of sharper peaks in the BBXRD data shown in Figure 1 (A), relative to the GIXRD data, suggests that the β -WC_{1-x} phase is more crystalline at the bottom layer of the thin-film, in agreement with literature^{7, 25} and suggesting that higher concentrations of carbon in the thin-film results in more nanocrystalline or amorphous β -WC_{1-x} precipitates. The multilayer structure of the as-deposited thin-film is shown in the STEM image from a cross-sectional lamella in Figure 1(B). A thin layer of the order of a few to tens of nm indicated by the yellow arrow, can be discerned at the substrate.

This may correspond to an amorphous layer generated by residual oxygen in the deposition chamber²⁷ and has been suggested to facilitate the adhesion of Cr to the substrate²⁷.

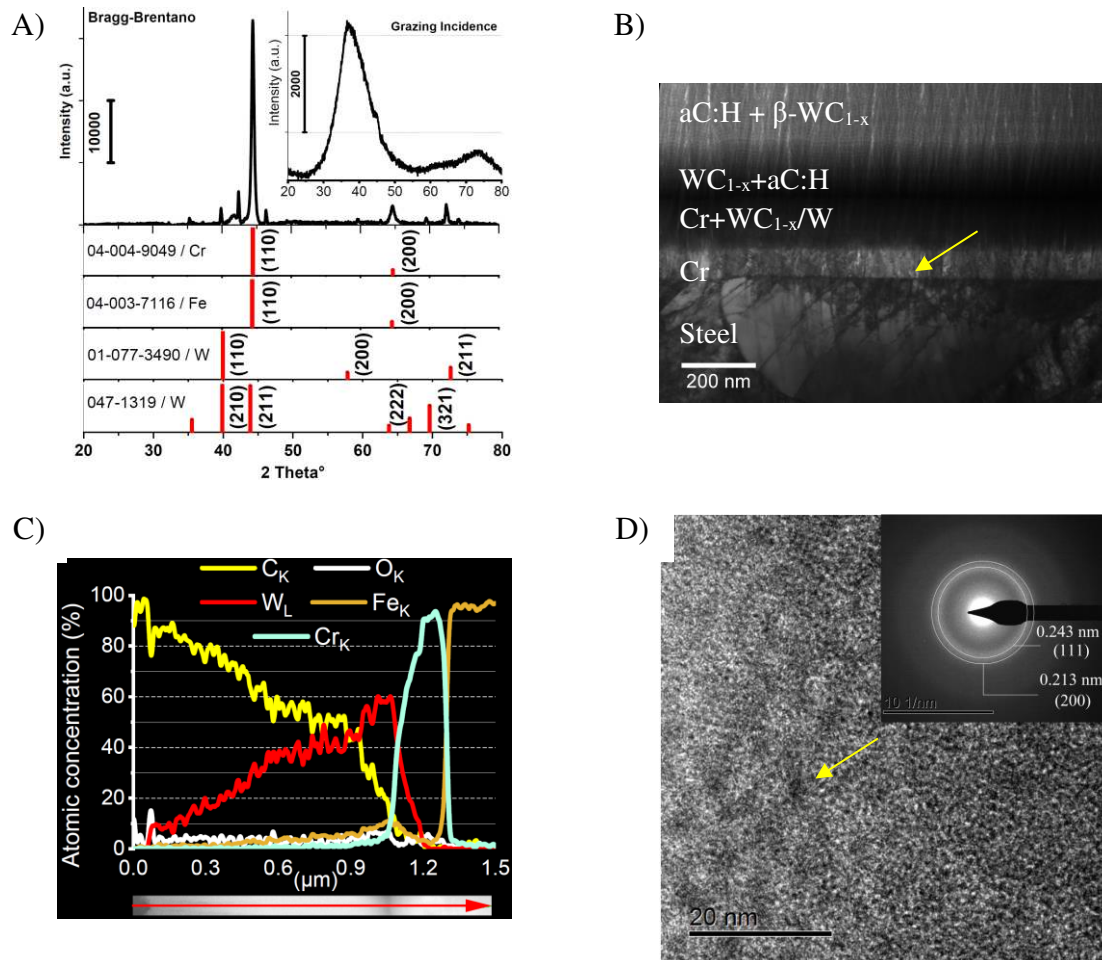


Figure 1. Structure and composition of WC/aC:H thin-film showing A) BB/GIXRD patterns from the thin-film (the peak in the BB-XRD pattern at $\sim 47^\circ$ can be attributed to Cr (211) plane which appears in Cr coatings²⁸), B) cross-sectional STEM image from the thin-film showing overview of the thin-film structure throughout its depth, C) STEM/EDX profile across the cross-sectional TEM lamella, traversing from the coating into the substrate (the rectangular bar below the EDX profile shows the corresponding STEM HAADF image from the profiled area) and D) HRTEM image and SAED pattern from the near-surface zone in the thin-film. Yellow arrows in (B) and (C) indicate an interfacial layer facilitating adhesion between the substrate and thin-film²⁷ and carbide nano-precipitates, respectively.

A STEM/EDX line profile across the lamella (Figure 1(C)) shows that the concentration of the alloyed-phase (W/WC) varies through the thin-film thickness as expected. Approximately 100 nm of the thin-film nearest to the substrate is a Cr interlayer sputtered in an argon plasma, followed by 150-200 nm of a simultaneously sputtered W/WC and Cr with an increasing concentration of W/WC over Cr. C_2H_2 gas was then introduced into the chamber to induce an aC matrix and the concentration of alloyed-phase was gradually reduced. Oxygen shows a

noticeable presence at the very top surface of the thin-film which is accompanied by a decrease in the relative concentration of carbon (Figure 1(C)). The residual pressure was maintained at the same level throughout the deposition and hence the enhanced presence of oxygen at the top surface of the film is due to atmospheric oxidation of the thin-film surface after it was taken out of the chamber. This oxidation is attributed to the formation of tungsten oxides and/or passivation of dangling bonds at the surface²⁹. A gradient of the alloyed-phase concentration is the preferred architecture yielding higher hardness in the film bulk (where there is a higher WC concentration) and improved friction and wear characteristics at the thin-film surface (where there is a higher aC concentration ($C > 60$ atom%) especially in humid environments³⁰.

A polycrystalline SAED pattern collected from approximately the top 100-nm of the thin-film is shown in Figure 1 (D) alongside a TEM image showing segregated nano-precipitates which index to the β -WC_{1-x} structure. In contrast, a SAED pattern collected from the bulk of the thin-film suggest a d spacing of 0.228 nm close to the (101) spacing in α -W₂C (shown in Figure S3). These observations agree with the findings of Sánchez-López et al.¹⁰ who showed that for phase fractions of WC > 66% in thin-films deposited by magnetron co-sputtering from graphite and WC targets, this induced the formation of α -W₂C, as opposed to β -WC_{1-x} which was formed at lower concentrations.

4.2 Fatigue mechanism in WC/aC:H thin films

Results in this section detail the wear mechanisms of the WC/aC:H thin-film lubricated with BO and BO+ZDDP under two SRRs of 2% and 10%. When ZDDP was present in the lubricant, the thin-film lubricated with a SRR of 2% (Figure 2 (A)) shows signs of mild polishing wear along with a few scratches on the surface (Figure 2 (A, a & b)); no micropitting was observed on the thin-film surface indicating a substantial improvement in micropitting performance as compared to steel surfaces (see Figure S4). Delamination of the thin-film was only observed on tested rollers on one occasion and this occurred at the interface between the Cr interlayer and the steel substrate (Figure 2 (A, c)). Increasing the SRR to 10% did not alter the wear mechanism significantly but enhanced the extent of damage; although no micropitting was observed, scratches became wider and a small degree of degradation wear was observed (Figure S5). Conversely thin-films lubricated with BO under a SRR of 2% exhibited sub-micron degradation wear and micropits on the surface, as seen in Figure 2 (B, a & b). Micropitting was observed both on the surface zone which experienced polishing wear (Figure 2 (B, b)) and also on the region where degradation wear occurred (Figure 2 (B, c)).

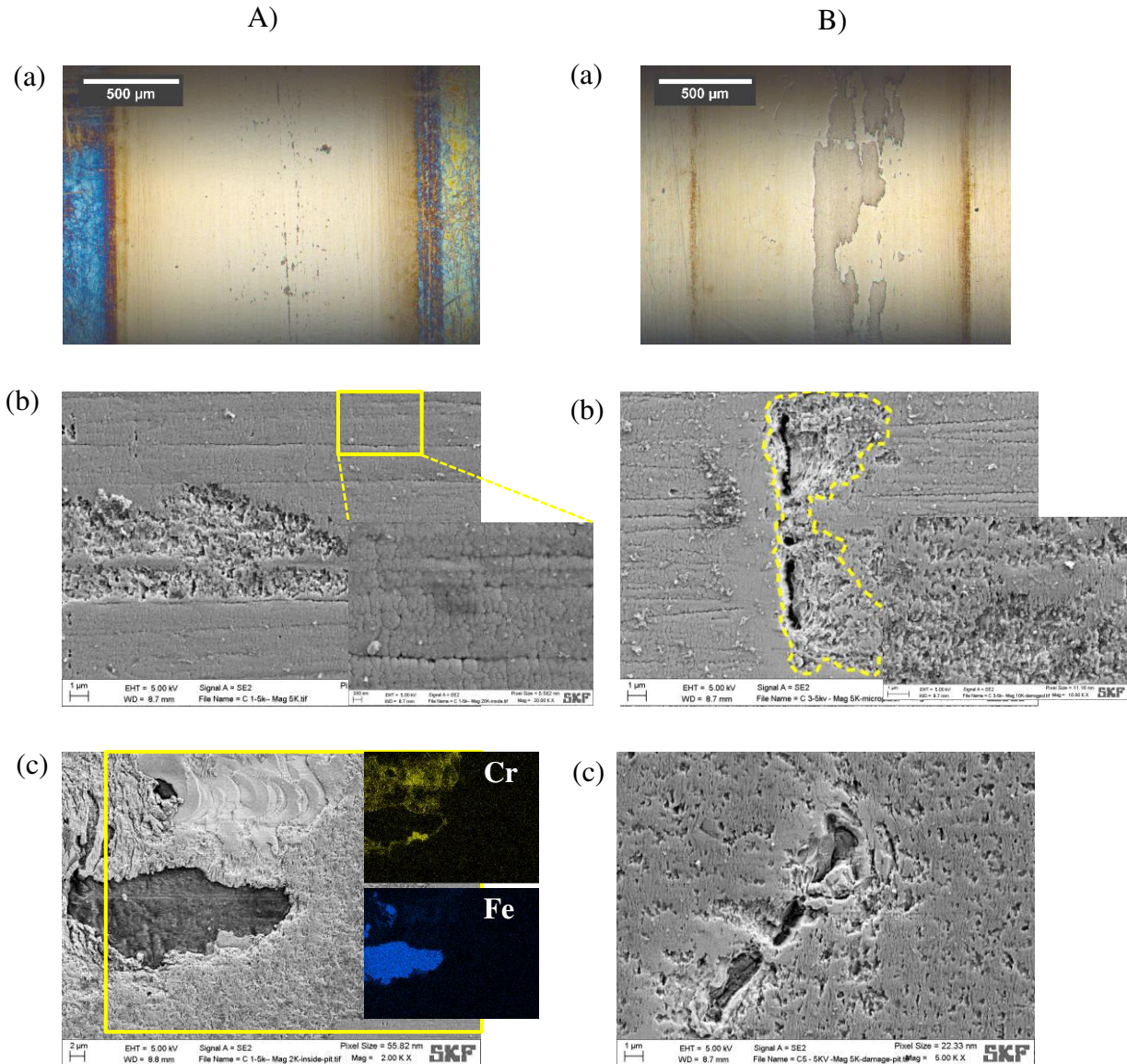


Figure 2. Micrographs from thin-film surfaces after tribo-contacts against steel-counterbodies, under 2% SRRs, at a contact pressure of 1.5 GPa and lubricated with A) BO+ZDDP and B) BO respectively. a) optical and b & c) secondary electron (SE) images showing superior micropitting-performance of the thin-film when ZDDP was present in the lubricant formulation. A,c) is a SE image showing localised delamination of the thin-film and its corresponding EDX elemental maps. Micropitting is indicated by yellow dash-line in panel B-b.

The wear scar on the thin-film showed a depth of 200-400 nm by WLI indicating significantly lower wear as compared to BO-lubricated steel surfaces (see Figure S4). The increase of SRR to 10% resulted in enhanced degradation wear and altered the appearance of micropits; in some cases micropits exhibited pothole shapes which can be an indication of a higher degree of micropit propagation in the circumferential direction (shown in Figure S5). Upon increase of the contact pressure to 2.5 GPa, spalling was observed on the thin-film surface lubricated with

BO+ZDDP together with polishing wear on the surface where the thin-film endured through the test. The spalling exhibited delamination of the thin-film from the substrate and is shown in Figure 3. Subsequent to delamination, micropits appeared on the steel surface.

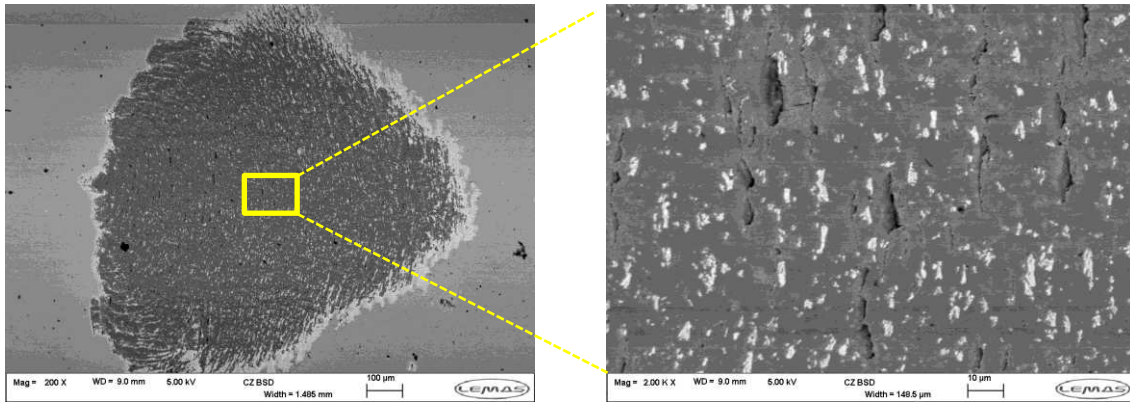


Figure 3. Back-scattered electron micrographs from thin-film surface after tribo-contact against steel-counterbodies using BO+ZDDP lubricant, under 2% SRR and at a contact pressure of 2.5 GPa showing spalling of the thin-film from substrate and micropits on the spalled surface. White spots in the inset and at the edge of the spall correspond to residual thin-film (mostly Cr interlayer) which were not worn away.

The coated surfaces lubricated with BO+ZDDP showed a similar friction behaviour to that of steel tests, alongside around 15% friction reduction as compared to steel surfaces (See Figure S4). The friction coefficient of coated surfaces lubricated with the base oil dropped rapidly during tribo-contact and was lower than that of BO+ZDDP lubricated thin-films (i.e. around 15%, see Figure S4). This behaviour is associated with carbonaceous transfer layer formation on the counter-body surfaces which has been shown to accompany friction reduction and high wear¹⁸. Conversely the friction coefficient of BO-lubricated steel surfaces was lower as compared to thin-film surfaces and BO+ZDDP lubricated steel surfaces. This was caused by severe solid-solid contacts at BO-lubricated steel surfaces leading to a significant reduction in the surface roughness of the counterbodies and a considerable change in the contact geometry and conformity resulting in decreased contact pressure³. A manifestation of the severe solid-solid contacts was a deep wear scar (Figure S4). ZDDP protected the steel surfaces from wear but induced micropits and high frictional forces on the steel surfaces (Figure S4) in agreement with the previous studies^{1,6}.

The fatigue mechanism of the thin-film was further investigated by preparing a TEM lamella from the thin-film lubricated with BO+ZDDP under a SRR of 2%. Figure 4 (A) shows a SEM image from the top surface of a pristine thin-film and Figure 4 (B) presents the thin-film surface after tribotesting using BO and a SRR of 2%. There are evident slit-like features on the surface

of the pristine thin-film which are denoted by yellow arrows in the figure. The slit-like features are defects which are generated during thin-film deposition. As seen in Figure 4 (C), these features can also be discerned in the cross-sectional electron micrographs of the pristine thin-film. The slit-like features in some cases extended throughout the thin-film which often, although not exclusively, appeared associated with polishing marks on the substrate surface.

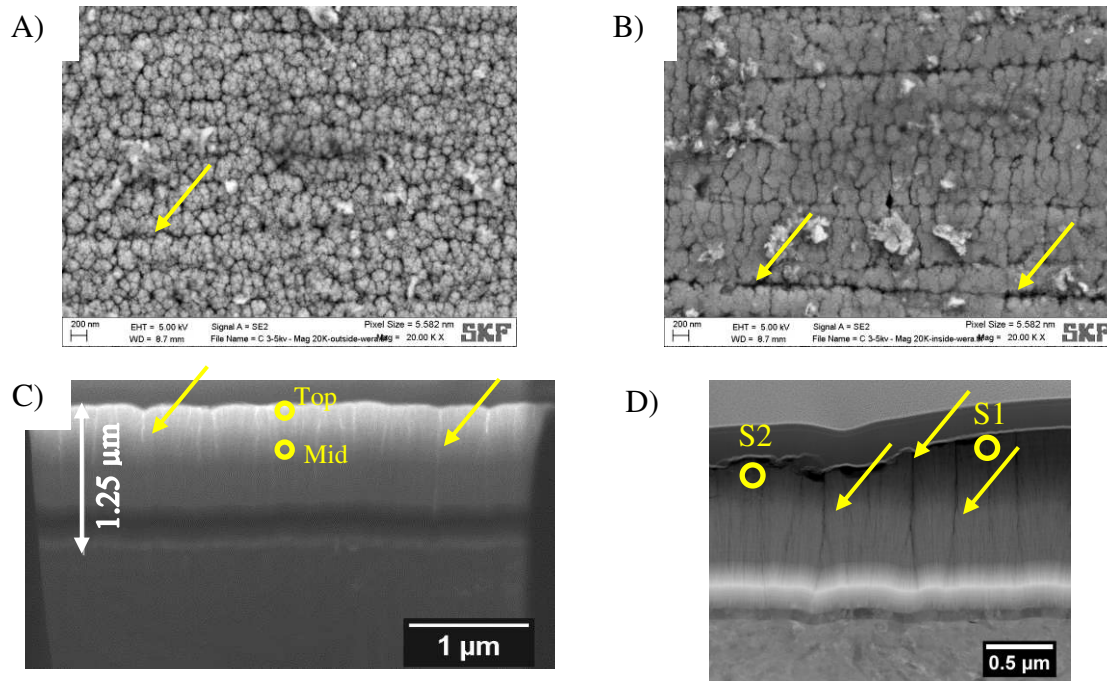


Figure 4. Plan view SEM (A and B) and cross-sectional (C and D) STEM images from (A) and (C) pristine unworn thin-film and (B) and (D) tribo-contacted thin-film against steel-counterbodies under 2% SRRs, at a contact pressure of 1.5 GPa and lubricated with BO+ZDDP respectively ((C) is a SEM image from a TEM lamella and (D) is a STEM HAADF image). Yellow circles in (C) and (D) S1 and S2, indicate the approximate locations from which EELS spectra in Figure 5 were collected.

Internal stresses, roller geometry (a barrel shape) and imperfections on the substrate are postulated to be contributing factors to slit generation. Wang et al.¹⁴ studied the influence of dopant concentration on internal stresses in WC-doped carbon thin-films and observed a narrow dopant concentration range in which intrinsic stress rises before dropping at higher concentrations. Therefore, the change in the concentration of β -WC_{1-x} at different thin-film depths results in varying residual stress behaviour and hence an increase in cohesive forces between layers which may be the driving force to dissociate the whole thin-film resulting in slit formation. The worn surface in Figure 4 (B) shows widening of the initial slits after tribo-contact and the cross-sectional STEM image in Figure 4 (D) confirms that surface damage originates from the initial slits. Therefore, defects on the thin-film surface act as damage

nucleation sites and hence the slits contribute to the factors leading to fatigue of the thin-film. As observed in Figure 2, ZDDP excelled in protecting the thin-film surfaces from micropitting. However, the slit widening and lamellar dissociation of the thin-film was observed following tribo-contact regardless of the lubricant formulation. Therefore, it can be inferred that ZDDP influences surface fatigue performance of the thin-film by chemically interacting with either carbon or β -WC_{1-x} in the thin-film which will be discussed in sections 4.3 and 4.4.

4.3 The carbon chemistry in the thin-film and the influence of ZDDP

4.3.1 EELS

The normalised C K-edge core loss EEL spectra collected from different areas (indicated in Figure 4) of the pristine thin-film and also the thin-film after tribo-testing using BO+ZDDP lubricant and a 2% SRR are shown in Figure 5. A reference C K-edge from an evaporated carbon layer which was deposited on the thin-film for surface protection is also included in Figure 5(A) for comparison. Three main features in the C K-edge are apparent: a first peak at 285.0 eV corresponds to transitions from the carbon 1s level to C=C π^* states, a second peak at 292 eV is attributed to C-C σ^* states and third peak at 300 eV is assigned to C=C σ^* states³¹. In addition, intensity in the region between the first two peaks, between ~ 286.6 and 288.5 eV²³, can arise from the presence of heterospecies (e.g. O and H bonded with carbon)³¹, non-planar sp^2 C-C bonds (similar to fullerene) and from the asymmetric tail of the π^* component^{23,31}. Furthermore, there will be a contribution from the carbide C K-edge associated with WC_{1-x} precipitates³² embedded in the aC:H matrix. The latter made reliable extraction of the carbon sp^2/sp^3 ratio from EELS C K-edge measurements extremely difficult owing to the varying WC alloying concentration as a function of depth within the thin-film.

As shown in Figure 5 (A), the C K-edge from the middle of the coating, with a higher concentration of WC, is almost identical to the C K-edge from the top of the coating where there is a lower alloying concentration and, in comparison with the C K-edge of evaporated carbon, both spectra show an increased relative intensity in the 286.6 eV to 288.5 eV region due to presence of C-H bonds. This implies that the a-C:H structure was not greatly affected by the change in the WC concentration which is in agreement with a prior report¹³. Also, this suggests that the contribution of β -WC_{1-x} to the total C K-edge intensity is small, at least for the upper and middle portions of the thin-film studied here, i.e. the number of carbon atoms associated with β -WC_{1-x} is in the minority as compared to the number of carbon atoms

associated with the aC:H matrix³². The overlaid spectra in Figure 5 (B) indicate that the structure and hybridisation state of the coating have not significantly altered following tribo-contact. However, a small change in the relative intensity can be observed in the energy region 286-289 eV. We attribute this to the presence of non-planar sp^2 bonds as reported for fullerenes³¹ and which has been observed in an a-C:H coating as a result of tribo-contact by Lanigan et al.²¹. In Figure 5 (B), the intensity of the sp^3 region (above 290 eV) remained relatively constant after tribo-contact which, if changes are occurring during wear, could imply a transformation of C–H bonds to non-planar sp^2 carbon bonds as has been observed in non-graphitising carbonaceous materials during heat treatment³¹.

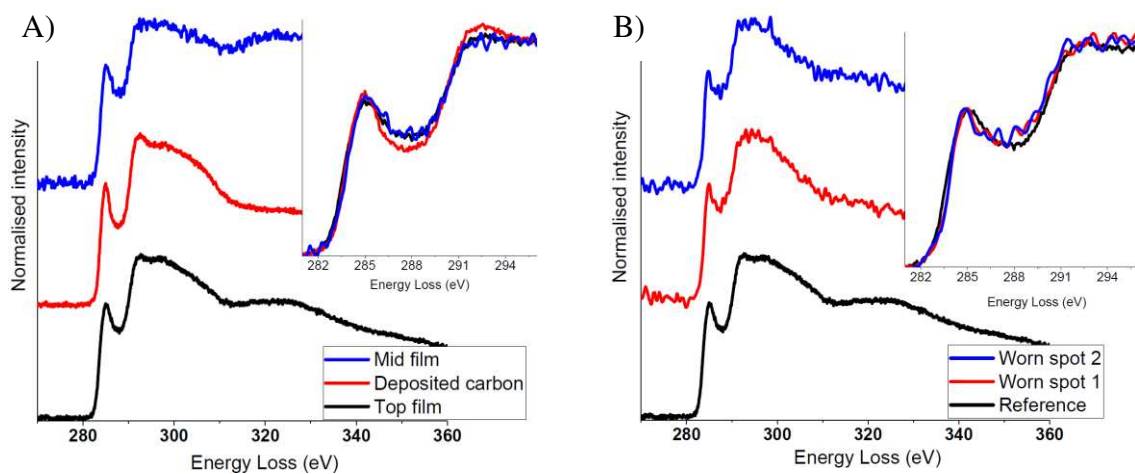


Figure 5. Core loss C K-edge spectra collected from A) pristine thin-film and deposited protective carbon layer on the thin-film and B) thin-film after tribo-contacts against steel-counterbodies, lubricated with BO+ZDDP under 2% of SRR and at a contact pressure of 1.5 GPa. The approximate locations associated with EELS spectra collection spots are shown in Figure 4 (C and D). Reference spectrum in (B) shows the C K-edge from the top of the pristine thin-film which is also presented in (A).

4.3.2 XPS and XAES from carbon

In Figure 6 (A) XPS C 1s spectra from three tribo-contacted thin-films are compared against a pristine surface. Deconvolution of all C 1s spectra led to an envelope of six peaks. The first peak at 283.6 eV is attributed to W and C bonding which is close to the binding energy (BE) values reported for cubic β -WC_{1-x} in the literature^{7, 33} and correlates with the GIXRD and SAED results. In contrast, the hexagonal carbide XPS C 1s peak is reported to be at \sim 282.8³⁴, a lower BE compared to the cubic phase^{7, 33}. The second intense peak at \sim 284.6 eV is associated with a-C:H carbon³⁵⁻³⁶ which is in the 284.4 - 284.6 eV BE range suggested by Kaciulis et al.³⁶. Adventitious aliphatic carbon gives rise to the third component at 285.0 eV³⁵⁻³⁶. The three remaining peaks at 286.6, 287.8-288.0 and 289.2-289.3 eV are minor

contributions which can be assigned to carbon-oxygen bonding³⁴. Full details of the C 1s XPS peak fitting and atomic concentrations associated with each component can be found in Table S3. It has been suggested that C–H bond formation results in a broadened XPS C 1s component³⁷. Here we observed that the FWHM of the a-C:H peak was reduced for tribo-contacted films relative to the pristine counterpart (Figure 6 (A)). This may suggest that the C–H bond contribution is diminished following tribo-contact which would be consistent with the observations derived from EELS.

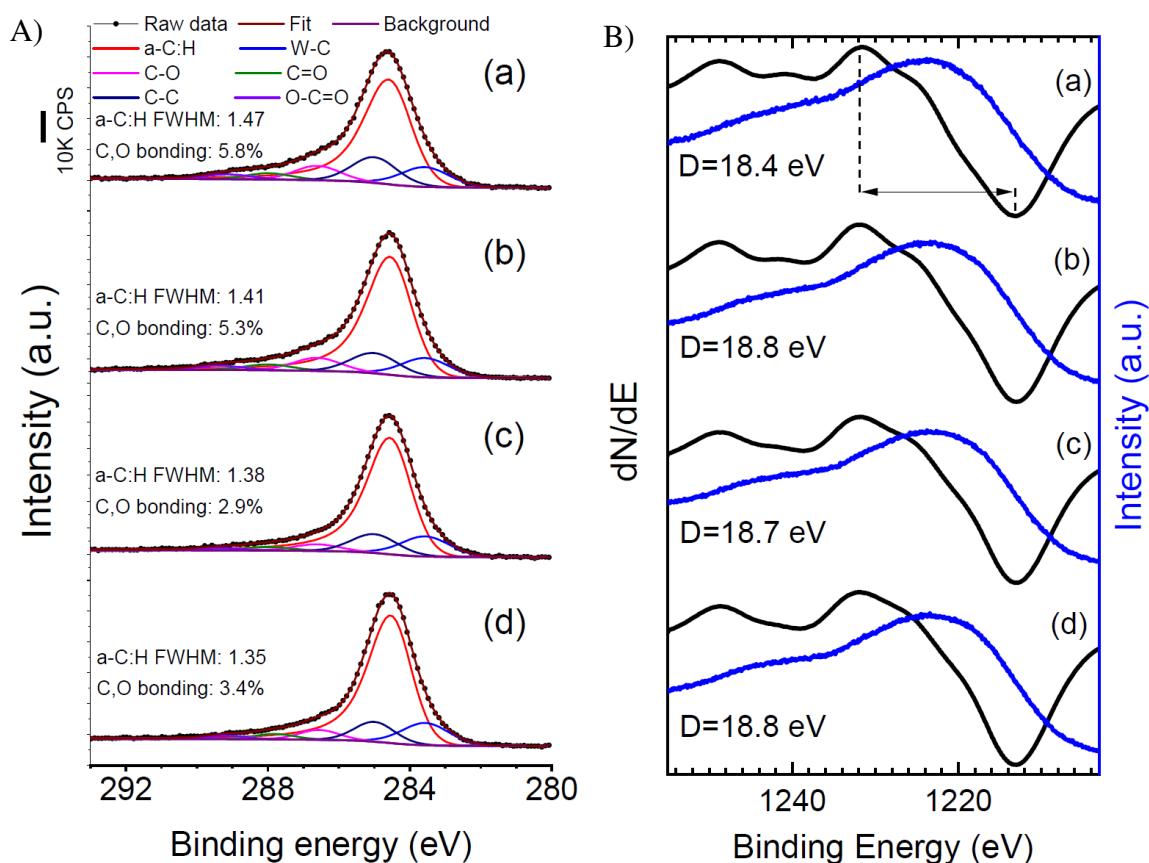


Figure 6. A) C1s XPS and B) C KVV XAES spectra collected from thin-film surfaces. Spectra present (a) pristine surface (b) the wear scar of the thin-film lubricated with BO under 1.5 GPa contact pressure and 2% of SRR (c) the wear scar of the thin-film lubricated with BO+ZDDP under 1.5 GPa contact pressure and 10% of SRR (d) the wear scar of the thin-film lubricated with BO+ZDDP under 2.5 GPa contact pressure and 2% of SRR. (b), (c) and (d) were collected from thin-film surfaces after tribo-contacts against steel-counterbodies.

Figure 6 (B) presents the X-ray excited C KVV Auger peaks and their first derivative signals from both pristine and tribo-contacted surfaces following in-situ cleaning using low energy Ar clusters which has been reported to remove contaminants without significant surface damage²⁴. The BE difference between the maximum and minimum points in the first derivative C KVV spectrum (the so-called D parameter) provides insight into the thin-film structure and has been

reported to be linearly proportional to the extent of sp^2 hybridisation in the carbon thin-film³⁸. The difference in D values observed for sp^2 graphite and sp^3 diamond is reported to be either 7.5 eV³⁶ or 8.3 eV³⁸. Following tribo-contact, the D parameter value increased by 0.3-0.4 eV (indicated in Figure 6 (B)), suggesting approximately a 5% change in hybridisation state (i.e. only a small increase in sp^2 bonding). With increasing H₂ flow during deposition, incorporation of H and O into the a-C:H has been shown to decrease the sp^2/sp^3 ratio due to the greater hydroxylic and carboxylic components on the surface³⁹. Therefore, as suggested by EELS and C 1s XPS results, it can be inferred that dehydrogenation of the thin-film, which results in dissociation of sp^3 C–H bonds and the formation of non-planar sp^2 C–C bonds, is the reason for the increase in D parameter for the tribo-contacted surfaces. This analysis assumes that the contribution of W–C bonds to C KVV Auger spectra remains unchanged and does not influence the D parameter calibration.

Features in the derivative C KVV spectra at ~1248 eV and ~ 1240 eV are attributed to a plasmon loss⁴⁰ and carbon-oxygen bonds³⁸ respectively. The C 1s XPS results in Figure 6 (A) show oxidised carbon species at the surface which decrease from 5.8 at% in the pristine thin-film to 2.9 at% in the thin-film tribo-contacted with BO+ZDDP and a 10% SRR ; this is also reflected in the intensity of the feature at ~1240 eV in the C KVV spectra. The other tribo-contacted thin-films also exhibited reductions in carbon-oxygen bonding as compared to the pristine thin-film. Reduction of C–O bonding has also been suggested to increase the D parameter^{38, 41} and this could be a potential mechanism for the observed change in carbon hybridisation state. However, at least in this case, the lowest contribution of C and O bonds (observed for the thin-film after tribo-contacts lubricated with BO+ZDDP and 10% SRR) does not associate with the largest D parameter. Accordingly, at least in this case, the change in C–H bonds appears to be the most influential factor leading to the observed increase in the D parameter.

4.4 Influence of the anti-wear additive

ZDDP is known to generate reaction films with a complex structure on both steel and amorphous-carbon coated surfaces^{17, 42}. Figure 7 (A) shows the XPS depth profile through the tribo-induced reaction film on the surface of the thin-film lubricated with BO+ZDDP. It shows a film composed of P, S, Zn and O, with S and P predominantly at the surface and O and, to a lesser extent Zn, extending deeper into the film. Some parameters from XPS analyses of the ZDDP-films on steel and thin film surfaces are presented in Table 1. As shown in Table 1,

ZDDP-derived films on the thin-film surface showed a similar Zn 3s - P 2p_{3/2} separation value to that of the film on the steel surface indicating a similar phosphate chain length⁴³. However, the modified Auger parameter (α') of the film on the amorphous carbon surface shifted to a lower value, close to the α' for ZnO which is reported to be 2009.5 – 2010.5 eV⁴⁴, implying a higher contribution of ZnO. Furthermore, in Table 1, slight, moderate and significant increases in the Zn/P, S/P and O/P atomic ratios respectively, were observed for the ZDDP-film on the WC/aC:H surface compared to the steel. This, together with the depth profile data, indicate that the reaction film is richer in oxidised compounds with potentially a multilayer structure comprising a ZnO-like layer at the interface between the thin-film surface and top phosphate-containing layer. STEM/EDX mapping was carried out on a thin film TEM cross-section which confirmed the presence of a Zn and O rich tribofilm at the interface (Figure S6). A multilayer ZDDP tribofilm structure has previously been reported⁴⁵ which suggested the presence of iron-oxide and iron/zinc sulphide/sulphate at the interface.

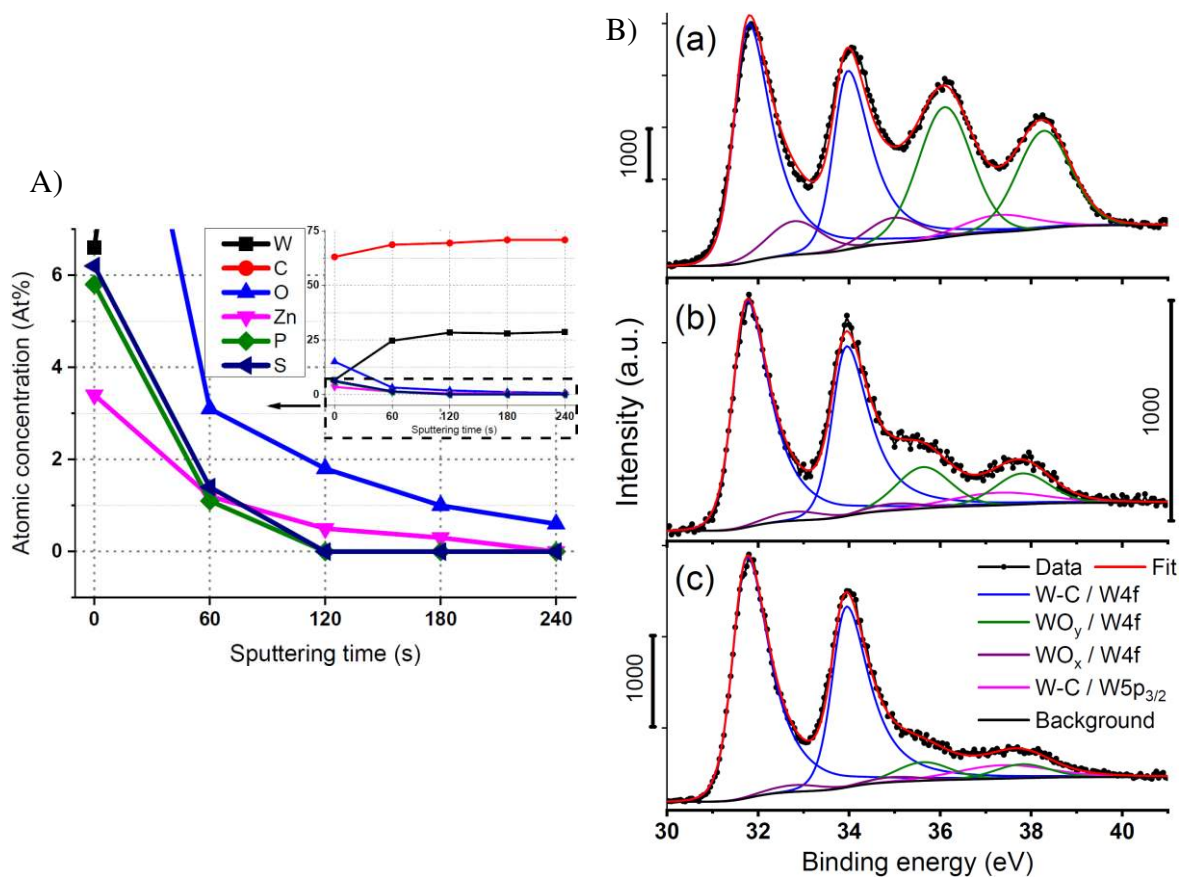


Figure 7. The influence of ZDDP additive on the surface chemistry of W-aC:H thin-films after tribo-contact against steel-counterbodies under 2% of SRR and at a contact pressure of 1.5 GPa. A) Depth profile of reaction film on the thin-film surface lubricated with BO+ZDDP, B) W 4f spectra collected from the top surfaces (prior to sputtering) of (a) the pristine thin-film, and tribo-contacted thin-films using (b) BO and (c) BO+ZDDP

XPS W 4f signals from both the pristine and tribo-contacted thin-film surfaces are presented in Figure 7 B(a-c) (Table S4). The W 4f peak was deconvoluted into seven peaks exhibiting three different valence states of W; six peaks are associated with the spin orbit splitting of the W 4f_{7/2} and 4f_{5/2} doublets (2.18 eV). The most intense peak at 31.7-31.8 eV can be assigned to the W 4f_{7/2} signal from metallic W and/or W-C bonding³⁴. As discussed in section 4.1, this peak corresponds to the β -WC_{1-x} phase^{7, 25, 33}. Note β -WC_{1-x} was deconvoluted using an asymmetric modified Lorentzian lineshape similar to Krasovskii et al.³³ which significantly influences the position and intensity of oxide peaks appearing with an energy shift relative to carbide phases. A carbide W 5p_{3/2} XPS signal appeared at 37.3-4 eV³⁴ showing a BE difference of ~5.5 eV relative to its corresponding W 4f_{7/2} core level which agrees with the BE difference (5.6 eV) reported for W⁰⁴⁶.

Fitting resulted in a peak at 32.8 eV which is assigned to a WO_x phase (x~2)⁴⁷⁻⁴⁸ corresponding to W in an oxidation state of IV^{34, 47} with a chemical shift of 0.9-1 eV relative to β -WC_{1-x}. An additional peak is present at either 36.1 eV or 35.6 eV in the pristine thin-film and the tribo-contacted surfaces respectively which can be assigned to WO_y where y is ~3. W 4f_{7/2} BE values of 35.5⁴⁷, 35.7⁸, 35.9⁴⁸ and 36.0⁴⁶ eV are attributed to the oxidation state VI (W⁶⁺). WO_x and WO_y compounds on the surface and indicate oxidised layers at the thin-film surface which are discernible in the STEM/EDX linescan in Figure 1 (C). Comparing the W 4f spectra in Figure 7 and Table S4 showing the atomic concentration of each component, it is clear that there is a substantial contribution of tungsten oxide to the chemistry of the surface film. The contribution of WO_y and WO_x dropped by 50% and 60% after tribo-contact in BO. In addition, the relative amount of WO_y on the thin-film surface lubricated with BO+ZDDP was less than half that on the BO lubricated surface indicating that the thin-film lubricated with BO+ZDDP had the least oxidised tungsten at the top surface.

Table 1. XPS parameters and atomic concentration ratio of elements detected in spectra acquisition. Spectra were collected from wear scars lubricated with BO+ZDDP under 2% of SRR and at a contact pressure of 1.5 GPa.

Test materials	Zn 3s - P 2p _{3/2}	Zn modified Auger parameter	Zn/P	S/P	O/P
Steel – Steel pair	6.85 ± 0.05 eV	2010.18 ± 0.12 eV	1.07	0.71	1.75
WC/aC:H–Steel pair	6.80 eV	2009.90 eV	1.09	1.00	2.99

5 Discussion

5.1 Impact of multilayer architecture and thin-film structure

We have shown that a multilayer β -WC_{1-x}-alloyed aC:H thin-film hinders micropitting on the roller bearing surfaces. A similar thin-film has been shown to enhance gear life, improve load carrying capacity by a factor of 200-300%² and provide promising corrosion resistance and low wear under dry contacts⁴⁹. Delamination of the thin-film is highly influenced by shear stresses at the subsurface region and was predominantly observed for a contact pressure of 2.5 GPa. The multilayer architecture has been shown to shift the depth of maximum shear stress closer to the top surface of the film⁴⁹ suppressing delamination from the substrate. This, however, induces stress localisation in the region closer to the top surface of the film resulting in micropitting, particularly for BO lubricated thin-films.

The role of the β -WC_{1-x} alloying-phase is to relax compressive internal stresses¹⁶, especially when in solid solution¹⁴, leading to a reduced potential for thin film delamination⁵⁰. A lower concentration of the alloyed-phase towards the thin-film surface results in smaller WC_{1-x} grains which results in smoother surfaces²⁶ so improving micropitting performance¹⁻² and hence a gradient in the alloying concentration is desirable. It is believed that a dispersion of tungsten carbide nanocrystallites in the amorphous matrix provides toughness¹⁶ and hence suppresses surface fatigue by inhibiting stress localisation. Localised stresses result in plastic deformation on the surface which triggers micropitting¹ and hence the presence of β -WC_{1-x} improves the thin-film properties accommodating shear stresses with minor surface damage during wear. .

With respect to the friction performance, BO+ZDDP-lubricated thin-films provided moderate friction reduction as compared to a steel-steel pair, with no significant damage to the thin-film surface. Although lubricious chemistries (e.g. WS₂) and/or graphitic compounds are postulated to form at the interfacial contact with WC/aC:H thin films resulting in friction reduction^{17, 19}, neither of these compounds were observed here. However tungsten oxides were observed at the outer surface of the thin film which may provide moderate friction reduction as a result of their enhanced propensity to shear (i.e. they possess solid lubricant properties)⁵¹. The aC:H thin film matrix underwent slight structural change during wear particularly for non-planar *sp*² C-C and *sp*³ C-H/O bonds, suggesting a tenacious structure for the WC/aC:H thin-film which is considerably harder than steel. This harder surface with a different chemical nature to the counterbody (i.e. steel) hinders adhesive wear between surfaces which in turn influences

frictional forces. Severe seizure and the incidence of pitting fatigue dramatically increase frictional forces in the contact ² and micropits on the steel surface act as stress concentration zones resulting in the evolution of areas at the surface which bear high localised contact pressures. At these areas, the lubricant film collapses resulting in an enhanced incidence of asperity-asperity contacts, so the proportion of load carried by the solid-solid increases. Accordingly, a thin-film surface with no micropits on the surface reduces solid-solid contacts leading to lower tangential forces.

5.2 Tribo-contact and changes in hybridisation state

Rehybridization of carbon sp^3 bonds to graphitic-like carbon sp^2 bonds within tribo-contacts has been postulated ⁵² to be the origin of low friction in carbon thin-films. Konicek et al. ²⁹ showed that the rehybridization of carbon sp^3 bonds promoted disordered carbon sp^2 bonding within sliding tribo-contacts which is then followed by wear of the softer sp^2 carbon-rich layer. They also postulated that repassivation of dangling bonds at surfaces brings about a friction reduction ²⁹.

In our studies we observed a relatively constant fraction of sp^3 C–C bonds, a slight increase in disordered non-planar sp^2 carbon bonding in agreement with some previous reports ^{21,29} and a possible decrease in C–H bonding (i.e. a dissociation of C–H bonds). We suggest that C–H bonds in the thin-film dissociated and re-hybridised to form disordered sp^2 carbon bonds. Cleavage of C–H bonds is favoured over C–C bonds ^{35, 53-54}, due to a significantly lower activation energy barrier for sp^3 C–H to sp^2 C–C bond transformation as compared to sp^3 C–C to sp^2 C–C transformation ³⁵ and sterically hindered access to sp^3 hybridised orbitals in C–C bonds ⁵³⁻⁵⁴. Interestingly we note that tungsten carbides have been shown to catalyse chemical reactions (including dehydrogenation) ⁵⁵. The superior wear/micropitting performance of the present coating may then originate from the maintenance of a stable and harder carbon sp^3 matrix (relative to sp^2) which resists tribo-induced shear stresses.

Thermal re-hybridisation of aC:H and taC structures have been shown in the literature ^{35, 56} showing sp^2 ordering of re-hybridised carbon bonds in aC:H at lower temperatures (just above 200°C) ³⁵ which was attributed to the incorporation of hydrogen into aC thin-films. Tribo-contact imposes frictional and shear forces on the thin-film which can be partly dissipated as heat, propelling C–H bond dissociation and the subsequent re-hybridisation. Tribo-induced shear forces have been postulated to reduce the activation energy of reactions ⁵⁷ and stretch

C–H bonds resulting in strain-driven cleavage triggered by mechanochemical energy⁵⁸. The tribo-induced re-hybridisation is probably a mechanism to compensate for tribo-stresses imposed on the thin-film similar to the dehydrogenation and re-arrangement to six-membered carbon rings observed by Catena et al.⁵⁹. Thermal effects usually involve ordered conformation of π electrons³⁵, while we observed formation of disordered sp^2 carbon bonds in agreement with some studies^{21,29} which could be due to the fact that shear stresses tend to increase entropy and plasticity. The formation of ordered hydrogenated sp^2 carbon structures following the dissociation of C–H bonds conferring super-lubricity on tribo-sheared aC:H contacts requires the existence of certain loading conditions⁶⁰. Therefore, the disordered sp^2 carbon bonds could be a transient response to tribostresses and could, in principle, transform to ordered sp^2 carbon bonds^{21,60} and/or re-hybridise (with the aid of mediators such as oleic acid for taC thin-films) and re-arrange to form (super)lubricious planar six-membered sp^2 rings²⁰.

5.3 Oxidation of the carbide phase and its influence on surface fatigue

The chemistry of the alloyed-phase at the very top layer of the pristine thin-film showed a significant oxide contribution (46 atomic%). Ellingham diagrams for the W, C and W,O binary systems show more negative values of free energy of formation (ΔG_f) for WO_2 and WO_3 as compared to WC and W_2C (see Table S5) implying the favoured formation of WO_3 . However, due to the low oxygen partial pressure in PECVD and plasma induced non-equilibrium, β - WC_{1-x} phase is formed in the thin-film. It is most likely that oxidation of the β - WC_{1-x} phase occurred post deposition forming an uppermost WO_y ($y \sim 3$) layer .

XPS results showed a BE decrease of 0.5 eV in WO_y following tribo-contact implying a reduction reaction of WO_y to sub-stoichiometric WO_{y-a} where $a < 1$ (e.g. $W_{18}O_{49}/W_5O_{14}/W_{24}O_{68}/W_{20}O_{58}$)⁶¹⁻⁶². Literature generally suggests oxidation during tribo-contact as opposed to reduction, however annealing of WO_3 at relatively high temperatures has been shown to induce oxygen vacancies in WO_3 resulting in a chemical shift of 0.6 eV to lower BE⁶³. It is also possible that crystallographic shear of the WO_3 structure could induce oxygen vacancies⁶⁴. Besides either thermal effects or crystallographic shear in tribo-contacts inducing oxygen-deficient WO_3 phases, alternatively tribo-oxidation of the exposed β - WC_{1-x} phase (following tribowear of the uppermost oxide layers) to sub-stoichiometric WO_{y-a} could occur. The stoichiometry and stability of the WO_{y-a} phase which formed as a result of tribo-contacts would be highly dependent on the oxygen accessibility at the thin-film surface. Although tribo-contacts were lubricated which should hinder oxygen access, the severe tribo-contact

conditions used in this study resulted in the collapse of lubricant films within contacting surface-asperities and hence potential exposure of the asperities to atmospheric oxygen and the generation of substantial heat dissipation into the contacting bodies.

Oxidation of the (WC) alloyed phase in aC thin-films has been shown to deteriorate their wear performance¹⁷. WO₃ has a large Pilling-Bedworth Ratio (PBR)^{62, 65} (3.39 - well above that of the oxides of Al, Ti and Cr) resulting in significant compressive stresses in the oxide layer⁶² which makes it susceptible to catastrophic delamination from the layer beneath, especially in regions of lattice mismatch. WO₃ shows several polymorphic phases depending on the temperature⁶⁶ and the stable phase at room temperature is monoclinic γ -WO₃ rather than the cubic crystal structure. Recurrent oxidation of β -WC_{1-x} to WO_{y-a}, may therefore result in a lattice mismatch and this, together with the large PBR value of WO_{y-a}, may result in continuing delamination of the oxide layer from the carbide phase under shear stress inducing the degradation wear observed on the thin-film surfaces, especially in the BO-lubricated surfaces which have a greater oxide contribution.

5.4 Influence of additive chemistry: suppression of oxidative fatigue

For the thin-films a higher friction coefficient was observed when ZDDP was present. This can be attributed to the formation of a ZDDP-tribofilm at the thin film surface which inhibits carbonaceous transfer-film formation⁶⁷. Conversely the ZDDP-tribofilm substantially improved the wear and fatigue performance of the thin-film (opposite to its effect on steel surfaces) which correlated with a reduction in oxide species at the thin-film surface. ZDDP, when subjected to thermal oxidation and tribostresses, generates a 50-200 nm thick film mainly comprised Zn/Fe (thio)phosphates on steel surfaces^{42, 45, 68-69}, which protects them from wear, together with minor traces of ZnO embedded between the phosphate chains, formed via the tribochemical reaction between polyphosphate and iron oxide⁴⁵. However, as is typical for aC coated surfaces, here we have shown a substantially thinner tribofilm (only 5-15 nm) containing minor traces of zinc phosphates at the top surface and a distinct ZnO layer (with a minor contribution of ZnS) at the interface between the phosphates and the as-deposited thin-film. The latter interfacial layer has not previously been reported in the literature and could arise as the product of either the reaction between ZDDP-induced polyphosphates and iron-oxide particles from the counterbody, or from the decomposition of basic ZDDP to neutral ZDDP and ZnO⁷⁰. Chemical digestion of the top oxide layer (WO₃) by polyphosphates from ZDDP to form ZnO is not envisaged, owing to the borderline Lewis acid characteristics of both

W^{6+} and Zn^{2+} . We note that a ZnO layer was not observed for an aC:H thin-film tested under the same conditions implying the catalytic impact of β -WC_{1-x} on ZDDP-film formation.

The suppressed oxidation of the β -WC_{1-x} phase (and the resultant reduced surface fatigue) when ZDDP was present in the lubricant can be explained by the antioxidant action of ZDDP molecules (which although well-known is not completely understood) and also the presence of dissociated ZnO from basic ZDDP which could act to inhibit hydrolysis reactions⁷⁰. In addition, the solid ZDDP-tribofilm can act as a physical barrier against inward diffusion of oxidative radicals.

Unlike XPS, STEM-EDX did not provide any great evidence for a phosphate-rich tribofilm suggesting that it may have been washed off during the cleaning procedure employed prior to FIB preparation. This would in turn imply a weakly bonded phosphate film at the very top layer of the tribofilm⁴². Zinc is believed to play an important role in facilitating crosslinking of the phosphate network under pressure⁶⁹ and the tribochemical decomposition of ZDDP to ZnO precipitates may have led to a Zn-deficient phosphate film so hindering its polymerisation and hence formation of a robust film^{42, 69}.

6 Conclusions

In this work the fatigue and wear mechanisms of a PECVD deposited WC/aC:H thin-film, composed of nanometre β -WC_{1-x} carbide precipitates dispersed in a sp^2/sp^3 bonded aC:H matrix at the top 100 nm of the film, were investigated using a variety of analytical techniques. Signs of a relatively more crystalline structure and cubic W/ α -W₂C were observed deeper in the thin-film where the phase fraction of the carbides increased. The formation of (and/or phase transformation to) a WO_{y-n} (and $n < 1$) layer after the tribological contact was observed, rather than initial WO_y ($y \sim 3$) phase at the pristine thin-film surface, implying the evolution of shear-induced oxygen vacancies. The results suggest a tribo-induced slight change to the hybridisation state of the aC:H matrix as transformation of carbon-hydrogen bonding to non-planar sp^2 carbon-carbon bonds, probably through rearrangements to closed loop carbon rings to compensate for shear stresses.

The ZDDP anti-wear additive which promoted micropitting on steel surfaces, actually mitigated against micropitting and alleviated degradative wear of the thin-film surfaces through formation of ZnO which assuaged oxidation of β -WC_{1-x}. The presence of ZDDP did not appear to influence the hybridisation state of the aC:H matrix. Conversely, the lowest friction

coefficient was observed with the base-oil only lubricant due to a greater formation of carbonaceous transfer film and lubricious tungsten oxide layers, whilst the thin-film suffered from micropitting and degradation wear. Increased contact pressure above the yield stress of the substrate led to delamination of the thin-film from the substrate, however, increasing the SRR to 10% did not alter the damage mechanism but intensified the extent of the damage. It was noted that ZDDP still remained effective in suppressing micropitting in the higher contact pressure and SRR.

7 Acknowledgments

This study was funded by the FP7 program through the Marie Curie Initial Training Network (MC-ITN) entitled “FUTURE-BET-Formulating an Understanding of Tribocorrosion in ArdUous Real Environments – Bearing Emerging Technologies” (317334) and was carried out at University of Leeds and SKF Engineering and Research Centre. The authors would like to thank to all FUTURE-BET partners whom had kind discussions on the topic and the methodology. The authors are grateful to Dr. Dave Doerwald and Mr. Ruud Jacobs from IHI Hauzer Techno Coating B.V for providing the study with the examined thin-films. The authors express their gratitude to Dr Michael B. Ward and Mr Stuart Micklethwaite from School of Chemical and Process Engineering, University of Leeds for the help with EELS/EDX-TEM spectra and image acquisitions. XPS data collection, presented in section 4.3.2, was performed at the EPSRC National Facility for XPS (‘HarwellXPS’), operated by Cardiff University and UCL, under contract No. PR16195.

8 Keywords:

Carbon thin-film, Tungsten carbide carbon coating, Tribochemistry, Micropitting, Surface fatigue, ZDDP, non-planar carbon ring, dehydrogenation

9 Supporting Information, a brief description:

Thin-film properties, a detailed description of the fatigue testing and its parameters (contact pressure and lubricant film calculations), analysis parameters and further supporting results including friction, SAED, XRD and STEM/EDX.

10 References

- (1) Lainé, E.; Olver, A. V.; Lekstrom, M. F.; Shollock, B. A.; Beveridge, T. A.; Hua, D. Y. The Effect of a Friction Modifier Additive on Micropitting. *Tribology Transactions* **2009**, *52* (4), 526-533.
- (2) Joachim, F.; Kurz, N.; Glatthaar, B. Influence of Coatings and Surface Improvements on the Lifetime of Gears. *Gear Technology* **2004**, *21* (4), 50-56.
- (3) Mahmoudi, B.; Doll, G. L.; Hager, C. H.; Evans, R. D. Influence of a WC/a-C:H Tribological Coating on Micropitting Wear of Bearing Steel. *Wear* **2016**, *350-351*, 107-115, DOI: <https://doi.org/10.1016/j.wear.2016.01.010>.
- (4) Moorthy, V.; Shaw, B. An Observation on the Initiation of Micro-Pitting Damage in as-Ground and Coated Gears During Contact Fatigue. *Wear* **2013**, *297* (1), 878-884.
- (5) Olofsson, U.; Sjöström, H.; Sjödin, U. Increased Wear Resistance of Roller Bearings Using Me-C: H Coated Rollers. *Journal of tribology* **2000**, *122* (4), 682-688.
- (6) Soltanahmadi, S.; Morina, A.; van Eijk, M. C.; Nedelcu, I.; Neville, A. Investigation of the Effect of a Diamine-Based Friction Modifier on Micropitting and the Properties of Tribofilms in Rolling-Sliding Contacts. *Journal of Physics D: Applied Physics* **2016**, *49* (50), 505302.
- (7) Voevodin, A. A.; O'Neill, J. P.; Prasad, S. V.; Zabinski, J. S. Nanocrystalline WC and WC/a-C Composite Coatings Produced from Intersected Plasma Fluxes at Low Deposition Temperatures. *Journal of Vacuum Science & Technology A* **1999**, *17* (3), 986-992, DOI: 10.1116/1.581674.
- (8) Abad, M. D.; Muñoz-Márquez, M. A.; El Mrabet, S.; Justo, A.; Sánchez-López, J. C. Tailored Synthesis of Nanostructured WC/a-C Coatings by Dual Magnetron Sputtering. *Surface and Coatings Technology* **2010**, *204* (21), 3490-3500, DOI: <https://doi.org/10.1016/j.surfcoat.2010.04.019>.
- (9) Voevodin, A. A.; Zabinski, J. S. Supertough Wear-Resistant Coatings with 'Chameleon' Surface Adaptation. *Thin Solid Films* **2000**, *370* (1), 223-231, DOI: [https://doi.org/10.1016/S0040-6090\(00\)00917-2](https://doi.org/10.1016/S0040-6090(00)00917-2).
- (10) Sánchez-López, J. C.; Martínez-Martínez, D.; Abad, M. D.; Fernández, A. Metal Carbide/Amorphous C-Based Nanocomposite Coatings for Tribological Applications. *Surface and Coatings Technology* **2009**, *204* (6), 947-954.
- (11) Scharf, T. W.; Romanes, M. C.; Mahdak, K. C.; Hwang, J. Y.; Banerjee, R.; Evans, R. D.; Doll, G. L. Atomic-Scale Structure and Composition of Tungsten Carbide Reinforced Diamondlike Carbon Films. *Applied Physics Letters* **2008**, *93* (15), 151909, DOI: 10.1063/1.2995860.
- (12) Monteiro, O. R.; Delplancke-Ogletree, M.-P.; Brown, I. G. Tungsten-Containing Amorphous Carbon Films Deposited by Pulsed Vacuum Arc. *Thin Solid Films* **1999**, *342* (1), 100-107, DOI: [https://doi.org/10.1016/S0040-6090\(98\)01441-2](https://doi.org/10.1016/S0040-6090(98)01441-2).
- (13) Wang, A.-Y.; Lee, K.-R.; Ahn, J.-P.; Han, J. H. Structure and Mechanical Properties of W Incorporated Diamond-Like Carbon Films Prepared by a Hybrid Ion Beam Deposition Technique. *Carbon* **2006**, *44* (9), 1826-1832.

- (14) Wang, A.-Y.; Ahn, H.-S.; Lee, K.-R.; Ahn, J.-P. Unusual Stress Behavior in W-Incorporated Hydrogenated Amorphous Carbon Films. *Applied Physics Letters* **2005**, *86* (11), 111902-111902.
- (15) Fallon, P. J.; Veerasamy, V. S.; Davis, C. A.; Robertson, J.; Amaratunga, G. A. J.; Milne, W. I.; Koskinen, J. Properties of Filtered-Ion-Beam-Deposited Diamondlike Carbon as a Function of Ion Energy. *Physical Review B* **1993**, *48* (7), 4777-4782, DOI: 10.1103/PhysRevB.48.4777.
- (16) Voevodin, A. A.; Prasad, S. V.; Zabinski, J. S. Nanocrystalline Carbide/Amorphous Carbon Composites. *Journal of Applied Physics* **1997**, *82* (2), 855-858, DOI: 10.1063/1.365784.
- (17) Yang, L.; Neville, A.; Brown, A.; Ransom, P.; Morina, A. Effect of Lubricant Additives on the WDLC Coating Structure When Tested in Boundary Lubrication Regime. *Tribology Letters* **2015**, *57* (2), 14, DOI: 10.1007/s11249-015-0464-y.
- (18) Podgornik, B.; Vižintin, J. Tribological Reactions between Oil Additives and DLC Coatings for Automotive Applications. *Surface and Coatings Technology* **2005**, *200* (5), 1982-1989, DOI: <https://doi.org/10.1016/j.surfcoat.2005.08.014>.
- (19) Yang, L.; Neville, A.; Brown, A.; Ransom, P.; Morina, A. Friction Reduction Mechanisms in Boundary Lubricated W-Doped DLC Coatings. *Tribology International* **2014**, *70*, 26-33.
- (20) Bouchet, M. I. D. B.; Martin, J. M.; Avila, J.; Kano, M.; Yoshida, K.; Tsuruda, T.; Bai, S.; Higuchi, Y.; Ozawa, N.; Kubo, M. Diamond-Like Carbon Coating under Oleic Acid Lubrication: Evidence for Graphene Oxide Formation in Superlow Friction. *Scientific Reports* **2017**, *7*, 46394.
- (21) Lanigan, J.; Freeman, Helen M.; Wang, C.; Ward, M. B.; Morina, A.; Neville, A.; Brydson, R. Understanding the Wear Behaviour of Non-Doped and Si,O-Doped Diamond-Like Carbon Films. *RSC Advances* **2017**, *7* (69), 43600-43610, DOI: 10.1039/C7RA08959G.
- (22) Strondl, C.; van der Kolk, G. J.; Hurkmans, T.; Fleischer, W.; Trinh, T.; Carvalho, N. M.; de Hosson, J. T. M. Properties and Characterization of Multilayers of Carbides and Diamond-Like Carbon. *Surface and Coatings Technology* **2001**, *142-144*, 707-713, DOI: [https://doi.org/10.1016/S0257-8972\(01\)01179-3](https://doi.org/10.1016/S0257-8972(01)01179-3).
- (23) Mironov, B. E.; Freeman, H. M.; Brown, A. P.; Hage, F. S.; Scott, A. J.; Westwood, A. V. K.; Da Costa, J. P.; Weisbecker, P.; Brydson, R. M. D. Electron Irradiation of Nuclear Graphite Studied by Transmission Electron Microscopy and Electron Energy Loss Spectroscopy. *Carbon* **2015**, *83*, 106-117, DOI: <https://doi.org/10.1016/j.carbon.2014.11.019>.
- (24) Morgan, D. J. Cluster Cleaned Hopg by XPS. *Surface Science Spectra* **2017**, *24* (2), 024003.
- (25) Pauleau, Y.; Gouy-Pailler, P. Characterization of Tungsten-Carbon Layers Deposited on Stainless Steel by Reactive Magnetron Sputtering. *Journal of Materials Research* **1992**, *7* (8), 2070-2079, DOI: 10.1557/JMR.1992.2070.
- (26) Baba, K.; Hatada, R.; Tanaka, Y. Preparation and Properties of W-Containing Diamond-Like Carbon Films by Magnetron Plasma Source Ion Implantation. *Surface*

and Coatings Technology **2007**, *201* (19), 8362-8365, DOI: <https://doi.org/10.1016/j.surfcoat.2006.02.086>.

(27) Evans, R. D.; Shiller, P. J.; Howe, J. Y. Adhesion of Tungsten Carbide Reinforced Amorphous Hydrocarbon Thin Films (WC/a-C:H) to Steel Substrates for Tribological Applications. *Journal of Applied Physics* **2011**, *109* (2), 023518, DOI: 10.1063/1.3544045.

(28) Quan, C.; He, Y. Properties of Nanocrystalline Cr Coatings Prepared by Cathode Plasma Electrolytic Deposition from Trivalent Chromium Electrolyte. *Surface and Coatings Technology* **2015**, *269*, 319-323, DOI: <https://doi.org/10.1016/j.surfcoat.2015.02.001>.

(29) Konicek, A.; Grierson, D.; Sumant, A.; Friedmann, T.; Sullivan, J.; Gilbert, P.; Sawyer, W.; Carpick, R. W. Influence of Surface Passivation on the Friction and Wear Behavior of Ultrananocrystalline Diamond and Tetrahedral Amorphous Carbon Thin Films. *Physical Review B* **2012**, *85* (15), 155448.

(30) Voevodin, A. A.; O'Neill, J. P.; Zabinski, J. S. Tribological Performance and Tribochemistry of Nanocrystalline WC/Amorphous Diamond-Like Carbon Composites. *Thin Solid Films* **1999**, *342* (1), 194-200, DOI: [https://doi.org/10.1016/S0040-6090\(98\)01456-4](https://doi.org/10.1016/S0040-6090(98)01456-4).

(31) Zhang, Z.-I.; Brydson, R.; Aslam, Z.; Reddy, S.; Brown, A.; Westwood, A.; Rand, B. Investigating the Structure of Non-Graphitising Carbons Using Electron Energy Loss Spectroscopy in the Transmission Electron Microscope. *Carbon* **2011**, *49* (15), 5049-5063, DOI: <https://doi.org/10.1016/j.carbon.2011.07.023>.

(32) Mohapatra, D. R.; Lee, H.-J.; Sahoo, S.; Lee, W.-S. A Novel Structure of Tungsten Carbide Nanowalls Grown on Nanocrystalline Diamond Film. *CrystEngComm* **2012**, *14* (6), 2222-2228, DOI: 10.1039/C2CE06161A.

(33) Krasovskii, P. V.; Malinovskaya, O. S.; Samokhin, A. V.; Blagoveshchenskiy, Y. V.; Kazakov, V. A.; Ashmarin, A. A. XPS Study of Surface Chemistry of Tungsten Carbides Nanopowders Produced through DC Thermal Plasma/Hydrogen Annealing Process. *Applied Surface Science* **2015**, *339*, 46-54, DOI: <https://doi.org/10.1016/j.apsusc.2015.02.152>.

(34) Moulder, J. F. Handbook of X-Ray Photoelectron Spectroscopy. *Physical electronics* **1995**, 230-232.

(35) Mangolini, F.; Rose, F.; Hilbert, J.; Carpick, R. W. Thermally Induced Evolution of Hydrogenated Amorphous Carbon. *Applied Physics Letters* **2013**, *103* (16), 161605.

(36) Kaciulis, S. Spectroscopy of Carbon: From Diamond to Nitride Films. *Surface and Interface Analysis* **2012**, *44* (8), 1155-1161, DOI: doi:10.1002/sia.4892.

(37) Dickrell, P. L.; Pal, S. K.; Bourne, G. R.; Muratore, C.; Voevodin, A. A.; Ajayan, P. M.; Schadler, L. S.; Sawyer, W. G. Tunable Friction Behavior of Oriented Carbon Nanotube Films. *Tribology Letters* **2006**, *24* (1), 85-90, DOI: 10.1007/s11249-006-9162-0.

(38) Lascovich, J.; Giorgi, R.; Scaglione, S. Evaluation of the sp²/sp³ Ratio in Amorphous Carbon Structure by XPS and XAES. *Applied Surface Science* **1991**, *47* (1), 17-21.

- (39) Caschera, D.; Cossari, P.; Federici, F.; Kaciulis, S.; Mezzi, A.; Padeletti, G.; Trucchi, D. M. Influence of PECVD Parameters on the Properties of Diamond-Like Carbon Films. *Thin Solid Films* **2011**, *519* (12), 4087-4091, DOI: <https://doi.org/10.1016/j.tsf.2011.01.197>.
- (40) Mizokawa, Y.; Miyasato, T.; Nakamura, S.; Geib, K. M.; Wilmsen, C. W. Comparison of the CKLL First-Derivative Auger Spectra from XPS and AES Using Diamond, Graphite, SiC and Diamond-Like-Carbon Films. *Surface Science* **1987**, *182* (3), 431-438, DOI: [https://doi.org/10.1016/0039-6028\(87\)90011-2](https://doi.org/10.1016/0039-6028(87)90011-2).
- (41) Barlow, A. J.; Popescu, S.; Artyushkova, K.; Scott, O.; Sano, N.; Hedley, J.; Cumpson, P. J. Chemically Specific Identification of Carbon in XPS Imaging Using Multivariate Auger Feature Imaging (Mafi). *Carbon* **2016**, *107*, 190-197, DOI: <https://doi.org/10.1016/j.carbon.2016.05.073>.
- (42) Gosvami, N. N.; Bares, J. A.; Mangolini, F.; Konicek, A. R.; Yablon, D. G.; Carpick, R. W. Mechanisms of Antiwear Tribofilm Growth Revealed in situ by Single-Asperity Sliding Contacts. *Science* **2015**, *348* (6230), 102-106, DOI: 10.1126/science.1258788.
- (43) Crobu, M.; Rossi, A.; Mangolini, F.; Spencer, N. D. Chain-Length-Identification Strategy in Zinc Polyphosphate Glasses by Means of XPS and ToF-SIMS. *Analytical and bioanalytical chemistry* **2012**, *403* (5), 1415-1432.
- (44) Dake, L.; Baer, D.; Zachara, J. Auger Parameter Measurements of Zinc Compounds Relevant to Zinc Transport in the Environment. *Surface and Interface Analysis* **1989**, *14* (1-2), 71-75.
- (45) Martin, J. M. Antiwear Mechanisms of Zinc Dithiophosphate: A Chemical Hardness Approach. *Tribology letters* **1999**, *6* (1), 1-8.
- (46) Olsson, C. O.; Mathieu, H. J.; Landolt, D. Angle-Resolved XPS Analysis of Molybdenum and Tungsten in Passive Films on Stainless Steel PVD Alloys. *Surface and Interface Analysis* **2002**, *34* (1), 130-134.
- (47) Katrib, A.; Hemming, F.; Wehrer, P.; Hilaire, L.; Maire, G. The Multi-Structure of Oxidized-Reduced Tungsten Carbide Surface (S). *Catalysis letters* **1994**, *29* (3-4), 397-408.
- (48) Sun, M.; Bürgi, T.; Cattaneo, R.; Prins, R. Tps, XPS, and QEXAFS Investigation of the Sulfidation Behavior of Tungsten on Fluorine-Promoted Alumina. *Journal of Catalysis* **2001**, *197* (1), 172-181.
- (49) Nemati, N.; Bozorg, M.; Penkov, O. V.; Shin, D.-G.; Sadighzadeh, A.; Kim, D.-E. Functional Multi-Nanolayer Coatings of Amorphous Carbon/Tungsten Carbide with Exceptional Mechanical Durability and Corrosion Resistance. *ACS applied materials & interfaces* **2017**, *9* (35), 30149-30160.
- (50) Shi, B.; Meng, W. J.; Rehn, L. E.; Baldo, P. M. Intrinsic Stress Development in Ti-C:H Ceramic Nanocomposite Coatings. *Applied Physics Letters* **2002**, *81* (2), 352-354, DOI: 10.1063/1.1492851.
- (51) Erdemir, A. A Crystal Chemical Approach to the Formulation of Self-Lubricating Nanocomposite Coatings. *Surface and Coatings Technology* **2005**, *200* (5-6), 1792-1796.

- (52) Wang, D.-S.; Chang, S.-Y.; Huang, Y.-C.; Wu, J.-B.; Lai, H.-J.; Leu, M.-S. Nanoscopic Observations of Stress-Induced Formation of Graphitic Nanocrystallites at Amorphous Carbon Surfaces. *Carbon* **2014**, *74*, 302-311, DOI: <https://doi.org/10.1016/j.carbon.2014.03.035>.
- (53) Sattler, A.; Parkin, G. Cleaving Carbon–Carbon Bonds by Inserting Tungsten into Unstrained Aromatic Rings. *Nature* **2010**, *463* (7280), 523-526.
- (54) Jones, W. D. The Fall of the CC Bond. *Nature* **1993**, *364* (6439), 676-677.
- (55) Hwu, H. H.; Chen, J. G. Surface Chemistry of Transition Metal Carbides. *Chemical reviews* **2005**, *105* (1), 185-212.
- (56) Grierson, D. S.; Sumant, A. V.; Konicek, A. R.; Friedmann, T. A.; Sullivan, J. P.; Carpick, R. W. Thermal Stability and Rehybridization of Carbon Bonding in Tetrahedral Amorphous Carbon. *Journal of Applied Physics* **2010**, *107* (3), 033523, DOI: 10.1063/1.3284087.
- (57) Spikes, H. Stress-Augmented Thermal Activation: Tribology Feels the Force. *Friction* **2018**, *6* (1), 1-31, DOI: 10.1007/s40544-018-0201-2.
- (58) Beyer, M. K.; Clausen-Schaumann, H. Mechanochemistry: The Mechanical Activation of Covalent Bonds. *Chemical Reviews* **2005**, *105* (8), 2921-2948.
- (59) Catena, A.; Guo, Q.; Kunze, M. R.; Agnello, S.; Gelardi, F. M.; Wehner, S.; Fischer, C. B. Morphological and Chemical Evolution of Gradually Deposited Diamond-Like Carbon Films on Polyethylene Terephthalate: From Subplantation Processes to Structural Reorganization by Intrinsic Stress Release Phenomena. *ACS applied materials & interfaces* **2016**, *8* (16), 10636-10646.
- (60) Chen, X.; Zhang, C.; Kato, T.; Yang, X.-a.; Wu, S.; Wang, R.; Nosaka, M.; Luo, J. Evolution of Tribo-Induced Interfacial Nanostructures Governing Superlubricity in aC: H and aC: H: Si Films. *Nature communications* **2017**, *8* (1), 1675.
- (61) Vasilopoulou, M.; Palilis, L. C.; Georgiadou, D. G.; Douvas, A. M.; Argitis, P.; Kennou, S.; Sygellou, L.; Papadimitropoulos, G.; Kostis, I.; Stathopoulos, N. A. Reduction of Tungsten Oxide: A Path Towards Dual Functionality Utilization for Efficient Anode and Cathode Interfacial Layers in Organic Light-Emitting Diodes. *Advanced Functional Materials* **2011**, *21* (8), 1489-1497.
- (62) Louro, C.; Cavaleiro, A. Thermal Oxidation of Tungsten-Based Sputtered Coatings. *Journal of the Electrochemical Society* **1997**, *144* (1), 259-266.
- (63) Diaz-Reyes, J.; Delgado-Macuil, R. J.; Dorantes-García, V.; Pérez-Benítez, A.; Balderas-Lopez, J. A.; Ariza-Ortega, J. Physical Properties Characterization of WO₃ Films Grown by Hot-Filament Metal Oxide Deposition. *Materials Science and Engineering: B* **2010**, *174* (1-3), 182-186.
- (64) Mohammad, A. A. J. A. P. P. A. Synthesis, Separation and Electrical Properties of WO₃-X Nanopowders Via Partial Pressure High Energy Ball-Milling. **2009**, *116* (2), 240-244.
- (65) Koch, F.; Brinkmann, J.; Lindig, S.; Mishra, T.; Linsmeier, C. Oxidation Behaviour of Silicon-Free Tungsten Alloys for Use as the First Wall Material. *Physica Scripta* **2011**, *2011* (T145), 014019.

- (66) Zheng, H.; Ou, J. Z.; Strano, M. S.; Kaner, R. B.; Mitchell, A.; Kalantar-zadeh, K. Nanostructured Tungsten Oxide—Properties, Synthesis, and Applications. *Advanced Functional Materials* **2011**, *21* (12), 2175-2196.
- (67) Equey, S.; Roos, S.; Mueller, U.; Hauert, R.; Spencer, N. D.; Crockett, R. Tribofilm Formation from ZnDTP on Diamond-Like Carbon. *Wear* **2008**, *264* (3), 316-321, DOI: <https://doi.org/10.1016/j.wear.2007.03.012>.
- (68) Guo, W.; Zhou, Y.; Sang, X.; Leonard, D. N.; Qu, J.; Poplawsky, J. D. Atom Probe Tomography Unveils Formation Mechanisms of Wear-Protective Tribofilms by ZDDP, Ionic Liquid, and Their Combination. *ACS applied materials & interfaces* **2017**, *9* (27), 23152-23163.
- (69) Mosey, N. J.; Müser, M. H.; Woo, T. K. Molecular Mechanisms for the Functionality of Lubricant Additives. *Science* **2005**, *307* (5715), 1612-1615, DOI: 10.1126/science.1107895.
- (70) Burn, A. J.; Dewan, S. K.; Gosney, I.; Tan, P. S. Inhibition of Hydrolysis of 'Normal'zinc (II) O, O'-Di-Isopropyl Dithiophosphate by the 'Basic'form. *Journal of the Chemical Society, Perkin Transactions 2* **1990**, (8), 1311-1316.